Journal Name

ARTICLE TYPE

Cite this: DOI: 00.0000/xxxxxxxxxx

Neither Sphere nor Cube - Analyzing the Particle Shape using Small-Angle Scattering and the Superball Model

Dominique Dresen,[a] Asmaa Qdemat,[a] Dominika Zákutná,[a†] Erik Wetterskog,[b‡] Emmanuel Kentzinger,[c] German Salazar-Alvarez,[b] and Sabrina Disch*[a]

Received Date
Accepted Date

DOI: 00.0000/xxxxxxxxxx

Accurate characterization of the nanocrystal shape with high statistical relevance is essential for exploiting the strongly shape-dependent properties of cuboidal nanoparticles towards applications. This work presents the development of a new small-angle scattering form factor based on the superball geometry. The superball quantifies the characteristic rounding of corners and edges of cuboidal nanoparticles with a single parameter. Applied to small-angle scattering data of sufficiently monodisperse nanoparticles, the superball form factor enables differentiation between the effects of extended particle size distribution and irregular particle shape. The quantitative application of the superball form factor is validated against microscopy data for a series of monodisperse nanoparticles and implemented into the user-friendly, open source software Sasview.

1 Introduction

With the progress in the synthesis and characterization of faceted nanoparticles of the last decades[1–3], the enormous potential of nanocrystal shape as a tuning knob for their physicochemical properties has become evident. The nanocrystal shape critically influences the optical[4,5], catalytic[6,7], magnetic[8–10], and orientational properties[11,12] and directs the symmetry of self-organized superlattices[13,14]. Nanocrystals with cubic morphology have attracted considerable interest for their symmetry-directing properties in self-organization towards mesocrystals with orientational order of their nanoscale building blocks[15–18], leading to directionally anisotropic physical properties such as charge transport[19] and magnetic anisotropy[20]. A surface curvature in between that of spherical and faceted particles critically affects the ligand binding[21] and the interparticle interactions of freely dispersed particles[22,23]. Consequently, even subtle deviations from the cubic morphology have a pivotal influence on the orientation and arrangement of both nanocrystals[24–26] and larger colloidal particles[27,28].

The precise specification of the nanoparticle shape is thus important to understand and predict their arrangement and physical properties. For nominally cubic nanoparticles, the characteristic blunted state of their corners has been described by a degree of truncation[24,25] or cubicity factor[29], which are both accessible from high-resolution electron microscopy data. Taking into account the roundness of the particle corners, the concept of a rounded cubic shape[30] has recently been reported as an intersection of a cube and a sphere.

The superball geometry describes a smooth transition between cubic and spherical morphologies with a simultaneous rounding of corners and edges. It is widely used in the theoretical description of nanocrystals and colloidal particles, where it has been applied as a model for electrical, hydrodynamic, and osmotic properties of cuboidal particle suspensions[31], particle packing[32–34], and dipolar interactions[35]. The superball particle shape has also been approximated by a combination of spheres with different sizes to model the interparticle interactions and macroscopic magnetic response of magnetic colloids[22,23,36]. Despite being well established in theoretical approaches, only a few experimental studies have applied the superball geometry to nanoparticles[26] and colloids[23,27,37,38].

Small-angle scattering techniques are routinely applied to the nanoparticle morphology including particle size and shape as well as size distribution, providing a global view of the sample with good statistics in a fast acquisition time[39]. The small-angle scattering by nominally cubic nanoparticles can technically be described using a spherical form factor by considering an overestimated particle size distribution resulting from the orientational average of nanocubes[9,25,40] or by a perfectly cubic form factor. For real samples, especially when the size distribution is narrow and the data quality is sufficient to resolve several form factor

[a]Department für Chemie, Universität zu Köln, Greinstr. 4-6, 50939 Köln, Germany. E-mail: sabrina.disch@uni-koeln.de
[b]Department of Materials Science and Engineering, Ångström Laboratory, Uppsala University, Box 35, 751 03 Uppsala, Sweden.
[c]Jülich Centre for Neutron Science JCNS, Peter Grünberg Institut PGI, JARA-FIT, Forschungszentrum Jülich GmbH, D-52425 Jülich, Germany.
† Current address: Charles University, Prague, Czech Republic.
‡ Current address: Vetenskapens Hus, Roslagstullsbacken 29, 114 21 Stockholm, Sweden.

minima in great detail, both form factors still deviate strongly from the experimental data, indicating an actual shape between that of a sphere and a cube[41]. A straight-forward approach towards characterization of small-angle scattering data of cuboidal nanoparticles with a quantitative description of the characteristic shape between a sphere and a cube is therefore needed and currently missing.

Here we present the superball form factor for a realistic description of the particle shape using small-angle scattering techniques. We establish the shape function that relates the superball parameters to parameters easily accessible from imaging experiments and derive the orientationally averaged form factor for evaluation of SAS data. The form factor is validated by comparing HRTEM and SAXS data for a series of iron oxide nanoparticles. For hands-on accessibility and wide-spread application, the orientationally averaged superball form factor has been implemented into the open source software SasView[42].

2 Model

2.1 Superball Shape Function

A superball is a geometric body that is in between a cube and a sphere, defined by the shape parameter p. The volume of a superball is defined by all points (x, y, z) that solve

$$x^{2p} + y^{2p} + z^{2p} < \left(\frac{a}{2}\right)^{2p}, \tag{1}$$

where a is the edge length of the superball. The case $p = 1$ is equivalent to the definition of a sphere with radius $r = \frac{a}{2}$ and the case $p = \infty$ corresponds to a cube.

To calculate the volume and radius of gyration of a superball, a transformation analogue to the spherical coordinate transformation helps to make use of the symmetries of the superball body by using modified spherical coordinates with $r = \frac{a}{2}$

$$x = r\cos^{p^{-1}}(\phi)\sin^{p^{-1}}(\theta), \tag{2}$$

$$y = r\sin^{p^{-1}}(\phi)\sin^{p^{-1}}(\theta), \tag{3}$$

$$z = r\cos^{p^{-1}}(\theta), \tag{4}$$

where ϕ and θ are the polar and azimuthal angles as defined for a sphere. The Jacobi determinant for the coordinate transformation in integral equations evaluates to

$$\det(J(x,y,z)) = \frac{r^2}{p^2}\sin^{p^{-1}}(\theta)\left(\cos(\phi)\sin(\phi)\cos(\theta)\sin(\theta)\right)^{p^{-1}-1}. \tag{5}$$

Using this transformation, the integral to determine the volume is given by

$$V = \frac{8}{p^2}\int_0^r r^2\mathrm{d}r\int_0^{\frac{\pi}{2}}\cos^{p^{-1}-1}(\phi)\sin^{p^{-1}-1}(\phi)\mathrm{d}\phi \int_0^{\frac{\pi}{2}}\cos^{p^{-1}-1}(\theta)\sin^{2p^{-1}-1}(\theta)\mathrm{d}\theta, \tag{6}$$

where only one octant needs to be explicitly integrated over. For the integrals over ϕ and θ the definition of Euler's Beta integral[43]

$$B(x,y) = 2\int_0^{\pi/2}\cos^{2x-1}(\alpha)\sin^{2y-1}(\alpha)\mathrm{d}\alpha, \tag{7}$$

and the identity with the gamma function

$$B(x,y) = \frac{\Gamma(x)\Gamma(y)}{\Gamma(x+y)} \tag{8}$$

is used to obtain

$$V = \frac{a^3}{12p^2}\frac{\Gamma^3\left(\frac{1}{2p}\right)}{\Gamma\left(\frac{3}{2p}\right)}. \tag{9}$$

The radius of gyration r_g, defined by the average square distance from the center of mass, is calculated by the integral

$$r_g^2 = \frac{1}{V}\int_V (x^2+y^2+z^2)\mathrm{d}^3r, \tag{10}$$

which is solved using the same coordinate transformation and identities as used to determine the volume and results in

$$r_g^2 = \frac{9a^2}{20}\frac{\Gamma^2\left(\frac{3}{2p}\right)}{\Gamma\left(\frac{1}{2p}\right)\Gamma\left(\frac{5}{2p}\right)}. \tag{11}$$

Looking at a superball in the plane $z = 0$, the diagonal d between two opposing rounded corners can be related to the edge length of the cube geometrically by

$$d = \sqrt{2}^{1-p^{-1}}a, \tag{12}$$

which yields an equation to determine p from an imaging experiment by

$$p = \frac{1}{1+2\log_2(a/d)}. \tag{13}$$

2.2 Superball form factor

For the form factor amplitude no analytic expression is known and therefore it needs to be solved numerically. For this purpose, cartesian coordinates provide the best setup for a fast and numerically stable algorithm of the amplitude of the oriented superball formfactor $p_{\text{orient.}}(\vec{q})$ for an arbitrary $\vec{q}$ direction

$$p_{\text{orient.}}(\vec{q}) = \frac{1}{V_p}\int_V \mathrm{d}\vec{r}e^{i\vec{q}\cdot\vec{r}} \tag{14}$$

$$= \frac{r^3}{V_p}\int_{-1}^{1}\mathrm{d}x\int_{-\gamma}^{\gamma}\mathrm{d}y\int_{-\zeta}^{\zeta}\mathrm{d}z e^{ir(q_x x+q_y y+q_z z)}, \tag{15}$$

$$= \frac{2r^2}{q_z V_p}\int_{-1}^{1}\mathrm{d}x\int_{-\gamma}^{\gamma}\mathrm{d}y e^{ir(q_x x+q_y y)}sin(rq_z\zeta), \tag{16}$$

with

$$\gamma = \sqrt[2p]{1-x^{2p}}, \tag{17}$$

$$\zeta = \sqrt[2p]{1-x^{2p}-y^{2p}}. \tag{18}$$

Splitting the integral into it's real and imaginary part using Euler's identity yields

$$\Re\mathrm{e}(p_{\mathrm{orient.}}(\vec{q})) = \frac{2r^2}{q_z V_p}\int_{-1}^{1}\mathrm{d}x\int_{-\gamma}^{\gamma}\mathrm{d}y\cos(rq_x x + rq_y y)\sin(rq_z\zeta), \tag{19}$$

$$\Im\mathrm{m}(p_{\mathrm{orient.}}(\vec{q})) = \frac{2r^2}{q_z V_p}\int_{-1}^{1}\mathrm{d}x\int_{-\gamma}^{\gamma}\mathrm{d}y\sin(rq_x x + rq_y y)\sin(rq_z\zeta). \tag{20}$$

Using $\sin(-x) = -\sin(x)$, the imaginary part vanishes and only the real part needs to be numerically calculated. The real part can be further transformed to

$$p_{\mathrm{orient.}}(\vec{q}) = \frac{8r^2}{q_z V_p}\int_0^1\mathrm{d}x\cos(rq_x x)\int_0^{\gamma}\mathrm{d}y\cos(rq_y y)\sin(q_z r\zeta), \tag{21}$$

from which the oriented form factor $P_{\mathrm{orient.}}(\vec{q}) = |p_{\mathrm{orient.}}(\vec{q})|^2$ is obtained. This form factor is subsequently integrated over all possible orientations and a possible size distribution to obtain the form factor $P(q)$ which describes the scattering pattern obtained from diluted nanoparticles in dispersion. The particle size distribution of choice Λ can be included by integrating

$$\bar{P}_{\mathrm{orient.}}(\vec{q}) = \int \mathrm{d}r\Lambda(r,\sigma_r)V_p^2 P_{\mathrm{orient.}}(\vec{q};r), \tag{22}$$

and the orientation distribution is performed by integrating over all possible $\vec{q}$ directions

$$P(q) = \frac{2}{\pi}\int_0^{\pi/2}\mathrm{d}\varphi\int_0^{\pi/2}\mathrm{d}\theta\sin(\theta)\bar{P}_{\mathrm{orient.}}(\vec{q}). \tag{23}$$

In this work, the normalized log-normal size distribution $\Lambda(r,\sigma_r)$ was applied according to

$$\Lambda(r,\sigma_r) = \frac{1}{\sqrt{2\pi}\sigma_r r}\exp\left[-\frac{1}{2}\left(\frac{\log(r)-\log(r_0)}{\sigma_r}\right)^2\right]. \tag{24}$$

When solving the five integrals numerically, great care has to be taken to make sure that on the one hand the integrals converge up to numerical precision and on the other hand the computational time stays in a reasonable time frame. For this work, the oriented form factor amplitude is evaluated numerically at the given q values by using the integration method DQAG from the fortran library QUADPACK. DQAG uses the adaptive Gauss-Kronrod quadrature algorithm and works reliably with functions on real numbers with double precision. The size distribution is evaluated using Gauss-Hermite quadrature. For the orientation distribution, the cube symmetry of the superball reduces the orientation averaging to angles $\varphi, \theta \in (0, 90^\circ)$ and thus $\Omega = \pi/2$. Those two integrals are then solved by applying a Gauss-Legendre quadrature rule.

The resulting form factor is multiplied with a scaling constant $I_0 = N/V$ and scattering contrast $\Delta\rho^2$ to respect the particle concentration and scattering contrast relative to the medium. The superball form factor has been integrated into the open source software SasView[42] and will be available from version 5.05.

3 Experimental

3.1 Nanoparticle synthesis

All nanoparticle samples analyzed in this study (S26, C086, C096, C136) have been part of prior studies[9,25,26,44]. The nanoparticles of spherical and cuboidal shape consist of iron oxide (γ-Fe_2O_3) and were synthesized by thermal decomposition of iron oleate precursors according to[44,45]. Detailed information on the synthesis protocols is given in[44].

3.2 Transmission Electron Microscopy

High-resolution bright field transmission electron microscopy (HR-TEM) was carried out on a JEOL JEM-2100 microscope. Details on the microscope and particle diameter determination can be found in[26]. In order to evaluate the shape parameter precisely, only those particles oriented with the nanocubes facet on the grid were taken into account as only these give access to the edge length and the face diagonal of the cubes. The mean size D and its standard deviation σ_D were obtained by fitting the corresponding histogram with a lognormal size distribution $\Lambda(D,\sigma_D)$ according to eq. (24). The shape parameter p was determined according to eq. (13).

3.3 Small-Angle X-ray Scattering

Small-angle X-ray scattering (SAXS) measurements were performed at the GALAXI instrument[46] at Forschungszentrum Jülich, Germany. An incident X-ray wavelength of Ga K_α with λ = 0.13414 nm and a beam size of 0.7 x 0.7 mm^2 were used. Air scattering of the X-ray beam is minimized by a fully evacuated flight path from the source to the two-dimensional position sensitive Pilatus 1M detector. SAXS measurements were carried out using two sample detector distances of 835 mm and 3535 mm, resulting in a wide range of the scattering wave vector of 0.005 Å^{-1} $< q <$ 0.5 Å^{-1}. Nanoparticle dispersions in toluene were sealed in quartz capillaries (Hilgenberg GmbH) with 1.5 mm diameter and 0.01 mm wall thickness. The typical exposure time was 15 minutes per sample and detector distance. The SAXS data was calibrated to absolute units using fluorinated ethylene propylene 1400 Å (d = 0.35 mm) as reference material and corrected for the background scattering contributions of the empty capillary and the pure solvent.

4 Results and Discussion

4.1 Influence of the shape parameter

The geometric shape of the superball with variation of the shape parameter p is presented in Fig. 1 along with a simulation of the shape-dependent form factor behavior. For a direct assessment of the influence of the shape parameter p on the form factor, the radius of gyration was kept constant at $r_g = 7.746$ nm, corresponding to that of a sphere with $r = 10$ nm and a perfect cube with $a = 15.5$ nm, and the form factor was normalized by the particle volume to fulfill the condition $P(Q=0)/V^2 = 1$. A lognormal particle size distribution of σ_r = 5% was applied for all simulations. Consistency of the superball form factor with a classical sphere and cube form factor was verified for the boundary condi-

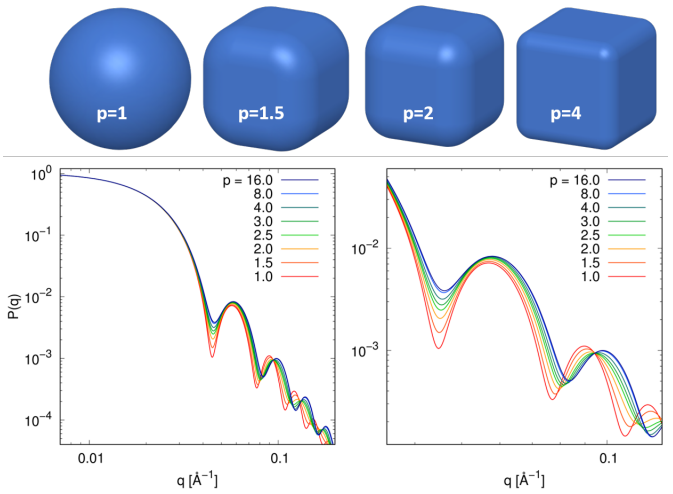

Fig. 1 Visualization of the superball shape for selected shape parameters p (top) and its corresponding form factor simulated for a particle size distribution of $\sigma_r = 5\%$ (bottom left), with a magnification of the first three form factor minima (bottom right).

tions of $p = 1$ and a large $p = 10000$, respectively. With increasing shape parameter p, a substantial variation of the form factor is observed. The first form factor minimum near $q = 0.045$ Å^{-1} exhibits a significant decrease in sharpness with increasing p, similar to the smearing effect of extended particle size distributions. In consequence, the SAXS by orientationally averaged nanocubes may be approximated by a spherical form factor at the expense of an overestimated particle size distribution as has been reported earlier[9,47]. The second and third form factor minima, however, exhibit an additional shape-dependent variation of their position in the scattering vector q as well as the relative scattering intensities. This behavior is distinct from the smearing that would result from enhanced particle size distributions and is therefore characteristic for the particle shape.

The superball form factor has clear advantages over the typical cubic and spherical form factors, if the particle size distribution is sufficiently narrow to resolve the second and third form factor minima experimentally. It promises an improved representation of SAXS or SANS data, including the higher-order minima with the aim to disentangle the effects of particle size distribution and particle shape and leading to a realistic description of the morphology of cuboidal nanoparticles. We note that the shape-dependent variation of the form factor is most evident for the smaller p values, promising a high sensitivity towards nanocubes with strongly rounded corners in the transition towards nanospheres.

4.2 Maghemite nanoparticles

For validation of the superball form factor against experimental SAXS data, four different nanoparticle samples of varying particle size and shape were investigated (Fig. 2a). The samples consist of maghemite ($\gamma - Fe_2O_3$) nanoparticles prepared by thermal decomposition and characterized in-depth in previous publications[9,25,26,44]. All samples exhibit a monodisperse particle size

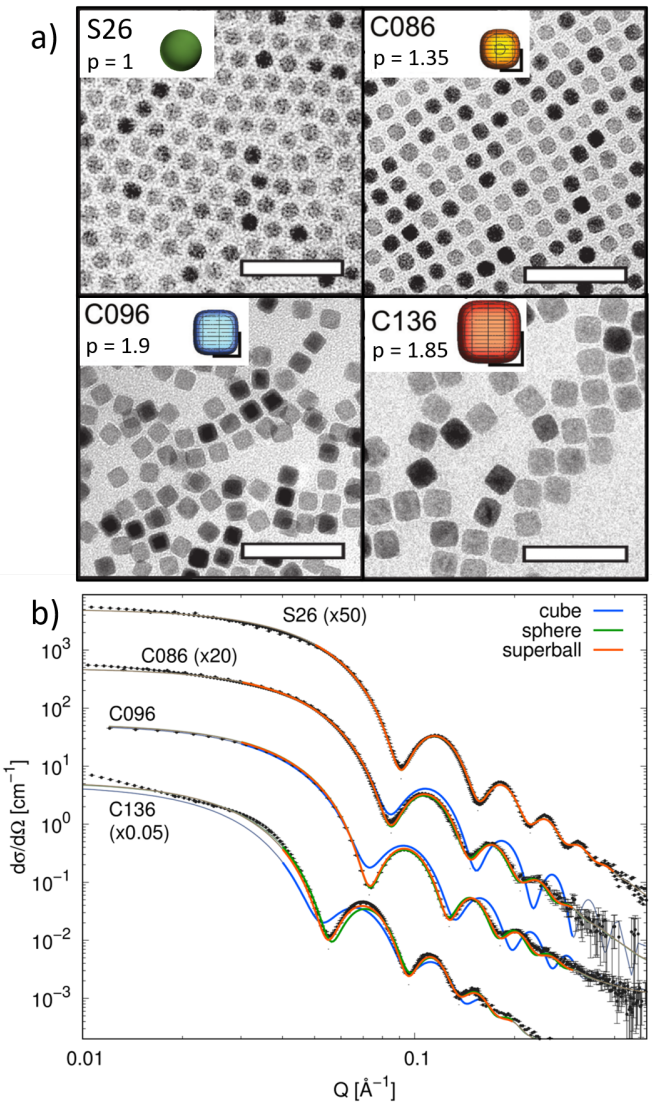

Fig. 2 a) Transmission Electron Microscopy (TEM) images of iron oxide nanoparticles with varying shape parameter p as determined from HRTEM. Scale bars: 50 nm. Adapted from[26,44]. b) Experimental Small-Angle X-ray Scattering (SAXS) by iron oxide nanospheres and nanocubes (symbols). Refinements using a cube, sphere, and superball form factor are shown. Color of the fit indicates the q range used for fitting, whereas grey lies indicate the form factors outside the fit ranges. Data scaled for clarity as indicated.

Table 1 SAXS refinement results of iron oxide nanospheres and nanocubes, compared to the superball morphology determined by HRTEM[26]. Shape parameter p, particle diameter $2R$ (sphere) and edge length a (superball) with lognormal size distribution σ are shown with reduced χ^2 and Akaike Information Criterion (AIC).

		SAXS		HRTEM
		sphere	superball	
S26	p	1	1.12(5)	1
	$2R = a$ [nm]	9.80(2)	9.5(1)	9.1(6)
	σ	6.66(6)%	6.6(1)%	
	χ^2_{red}	479	477	
	AIC	1774	1774	
C086	p	1	1.43(6)	1.35
	$2R = a$ [nm]	10.50(2)	9.56(8)	8.6(5)
	σ	7.1(1)%	6.5(2)%	
	χ^2_{red}	40.6	37.1	
	AIC	1077	1052	
C096	p	1	1.49(2)	1.90
	$2R = a$ [nm]	12.16(1)	11.00(2)	9.6(5)
	σ	6.2(1)%	5.4(1)%	
	χ^2_{red}	20.8	5.8	
	AIC	689	401	
C136	p	1	1.62(1)	1.85
	$2R = a$ [nm]	15.86(1)	14.40(1)	13.6(8)
	σ	6.8(1)%	5.7(1)%	
	χ^2_{red}	6895	5827	
	AIC	1612	1582	

distribution, which is required to resolve the second and third form factor minima using SAXS. In detail, the studied samples include conventional spherical (S26) as well as cuboidal nanoparticles (C086, C096, C136) with varying particle size and shape parameters in the range of 1.4-1.9 as determined from HRTEM images. As previously described, the here-in developed form factor seems to be sensistive to subtle variations of the cubic shape in the range $1 < p < 2$. In the following, we show that this is indeed the case.

SAXS data by all four samples are presented in Fig. 2b along with form factor refinements according to a classical sphere (p = 1), approximating a classical cube (p = 10000), and the superball form factor. For all cubic samples, the classical cube form factor clearly does not describe the data adequately. This is visible both from the misrepresented smearing of the first three form factor minima and from the position mismatch of the second and third form factor minima along the scattering vector q. This observation is in agreement with the TEM result of relatively small shape parameters p for all samples, corresponding to a significant rounding of the corners.

Refinement results using a sphere and superball form factor are listed in Table 1. For the spherical nanoparticles, S26, the fits using sphere and superball are equivalent as indicated by both the obtained statistical criteria (χ^2_{red} and AIC) and the fit results. The obtained shape parameter of $p = 1.12(5)$ approaches $p = 1$ within the uncertainties, and both fits coincide with each other and the data in Figure 2b.

For all nanocube samples C086, C096, and C136, the superball form factor leads to an improved fit of the SAXS data as judged

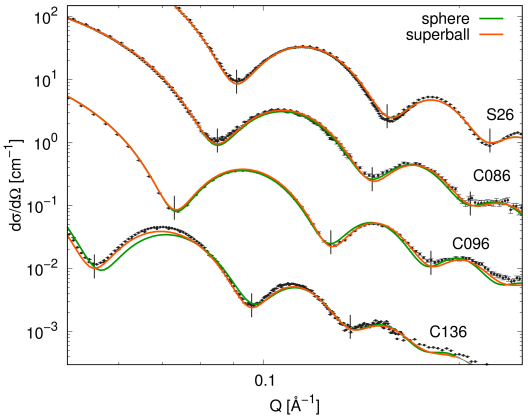

Fig. 3 Small-Angle X-ray Scattering (SAXS) by iron oxide nanospheres and nanocubes, refined using a sphere and superball form factor. Detail of Fig. 2b. The first three form factor minima in the experimental data are indicated with a vertical marker.

by the obtained χ^2_{red} and the Akaike Information Criterion as well as the visual inspection of the data and fits. A detailed view of the SAXS refinements presented in Figure 3 shows that the superball form factor, as opposite to the sphere form factor, describes well the position of the first three form factor minima, resulting in an improved fit to the data. The determined shape parameters p listed in Table 1 agree relatively well with those determined from HRTEM. For the more cubic nanoparticles C096 and C136, the HRTEM p is slightly larger than the superball fit result. This is attributed to the selection of particles to be measured using HRTEM, as the superball shape can only be determined directly for nanoparticles with their 001 zone axis aligned with the beam direction. Therefore, a certain degree of bias towards the more cubic nanoparticles, with flat facets that have a higher tendency to lie flat on the carbon film of the TEM grid, is hard to avoid. Such bias is absent for SAXS measurements, where a large number of nanoparticles (typically in the range of 10^{13} nanoparticles) is probed simultaneously independent of their orientation in the dispersion medium, c.f. TEM measurements where the typical number of particles used is about $10^1 - 10^2$. In addition, the need to calibrate the TEM magnification scale at each magnification results in slight errors in the size determination (a few percent units in the best cases). Therefore, the determination of p using the superball form factor is considered more accurate and precise than the determination of p by HRTEM.

The obtained superball edge lengths presented in Table 1 appear slightly larger than those determined from HRTEM. When translating the refined particle edge length a and lognormal size distribution σ_{log} into the mean and standard deviation, superball edge lengths of 9.6(6) nm (C086), 11.0(6) nm (C096), and 14.5(8) nm (C136) are derived, all of which are in reasonable agreement with the HRTEM results (Table 1). A number of reasons may be responsible for these discrepancies (in decreasing order of importance): i) Aging and topotactic oxidation of the samples is most likely, as the larger nanoparticles are known to consist of a wüstite-like core and a spinel-type shell in the pris-

tine state. The oxidation drives Fe(II) ions to the surface which increases the particle size and although the particle morphology is largely preserved[48] a slight rounding of the cube corners occurs. ii) Sampling bias may also be present, as the larger particles tend to agglomerate more and this agglomeration may result in losing the alignment of the zone axis with the electron beam. iii) Electron beam-induced transformation of such particles has been observed, where the local heating results in an increased ordering of vacancies in the nanoparticles and a subsequent lattice contraction, reducing slightly their particle size[49].

Effect i) is a priori dominant as the full oxidation of wüstite to maghemite is accompanied by a volume expansion of about 30%, in line with the obtained results. This is reasonable for the samples presented here, as the HRTEM measurements were typically performed on very fresh samples, whereas the SAXS was measured after several years, with enhanced statistics and resolution as needed for this study.

5 Conclusions

We have demonstrated how the superball form factor clearly disentangles the different effects of extended size distribution and variation of the shape on the smearing and q position of the form factor minima. We find a high sensitivity of the superball form factor to small p values, corresponding to strongly rounded cubes. This is the range of the transition between cubes and spheres, where even subtle variations of the particle morphology can have a profound influence on materials properties. The high sensitivity to small changes in p will also enable systematic and precise studies of the potential variation in particle shape in response to ageing effects or intraparticle reactions.

With our development of the superball form factor for small-angle scattering, a quantitative description of the transition between cubic and spherical shape of nanoparticles and colloids becomes accessible. The superball shape parameter p serves as a quantity for the characteristic rounding of the corners and edges and can be reliably determined from small-angle scattering data resolving the first two to three form factor minima.

We have validated the superball form factor against experimental SAXS data and confirm a good agreement of both particle size and shape parameter with those previously determined by HRTEM. The superball form factor thus provides a fast analysis of the geometrical shape of cuboidal nanoparticles and colloids with random orientation and high statistics.

Quantitative shape analysis using the superball form factor will help with the investigation of the impact of nanocrystal or colloidal shape on interparticle interactions, orientational alignment, surface chemistry and more, highly relevant in the broad field of the nanosciences.

Conflicts of interest

There are no conflicts to declare.

Acknowledgements

This work benefited from the use of the SasView application, originally developed under NSF award DMR-0520547. SasView contains code developed with funding from the European Union's Horizon 2020 research and innovation programme under the SINE2020 project, grant agreement No 654000. GSA was financially supported by the Swedish Research Council, VR (Research grant 2016-06959). Financial support from the German Research Foundation (DFG: Emmy Noether Grant DI 1788/2-1) is gratefully acknowledged.

Notes and references

1 C. Burda, X. Chen, R. Narayanan and M. A. El-Sayed, *Chem. Rev.*, 2005, **105**, 1025–1102.

2 Y. Xia, Y. Xiong, B. Lim and S. E. Skrabalak, *Angew. Chem. Int. Ed.*, 2009, **48**, 60–103.

3 Y. Xia, X. Xia and H.-C. Peng, *J. Am. Chem. Soc.*, 2015, **137**, 7947–7966.

4 K. L. Kelly, E. Coronado, L. L. Zhao and G. C. Schatz, *J. Phys. Chem. B*, 2003, **107**, 668–677.

5 M. Rycenga, C. M. Cobley, J. Zeng, W. Li, C. H. Moran, Q. Zhang, D. Qin and Y. Xia, *Chem. Rev.*, 2011, **111**, 3669–3712.

6 R. Narayanan and M. A. El-Sayed, *Nano Lett.*, 2004, **4**, 1343–1348.

7 S. Mostafa, F. Behafarid, J. R. Croy, L. K. Ono, L. Li, J. C. Yang, A. I. Frenkel and B. R. Cuenya, *J. Am. Chem. Soc.*, 2010, **132**, 15714–15719.

8 G. Salazar-Alvarez, J. Qin, V. Šepelák, I. Bergmann, M. Vasilakaki, K. N. Trohidou, J. D. Ardisson, W. A. A. Macedo, M. Mikhaylova, M. Muhammed, M. D. Baró and J. Nogués, *J. Am. Chem. Soc.*, 2008, **130**, 13234–13239.

9 S. Disch, E. Wetterskog, R. P. Hermann, A. Wiedenmann, U. Vainio, G. Salazar-Alvarez, L. Bergström and T. Brückel, *New J. Phys.*, 2012, **14**, 013025.

10 Z. Zhao, Z. Zhou, J. Bao, Z. Wang, J. Hu, X. Chi, K. Ni, R. Wang, X. Chen, Z. Chen and J. Gao, *Nat Commun*, 2013, **4**, 2266.

11 D. Hoffelner, M. Kundt, A. M. Schmidt, E. Kentzinger, P. Bender and S. Disch, *Faraday Discuss.*, 2015, **181**, 449–461.

12 D. Zákutná, Y. Falke, D. Dresen, S. Prévost, P. Bender, D. Honecker and S. Disch, *Nanoscale*, 2019, **11**, 7149–7156.

13 M. A. Boles, M. Engel and D. V. Talapin, *Chem. Rev.*, 2016, **116**, 11220–11289.

14 J. J. Geuchies, C. van Overbeek, W. H. Evers, B. Goris, A. de Backer, A. P. Gantapara, F. T. Rabouw, J. Hilhorst, J. L. Peters, O. Konovalov, A. V. Petukhov, M. Dijkstra, L. D. A. Siebbeles, S. van Aert, S. Bals and D. Vanmaekelbergh, *Nature Mater*, 2016, **15**, 1248–1254.

15 L. Bergström, E. V. Sturm, G. Salazar-Alvarez and H. Cölfen, *Acc. Chem. Res.*, 2015, 12.

16 E. V. Sturm and H. Cölfen, *Chem. Soc. Rev.*, 2016, **45**, 5821–5833.

17 J. J. Choi, K. Bian, W. J. Baumgardner, D.-M. Smilgies and T. Hanrath, *Nano Lett.*, 2012, **12**, 4791–4798.

18 Z. J. Urbach, S. S. Park, S. L. Weigand, J. E. Rix, B. Lee and C. A. Mirkin, *Angew. Chem. Int. Ed.*, 2021, **60**, 4065–4069.

19 A. Maier, D. Lapkin, N. Mukharamova, P. Frech, D. As-

salauova, A. Ignatenko, R. Khubbutdinov, S. Lazarev, M. Sprung, F. Laible, R. Löffler, N. Previdi, A. Bräuer, T. Günkel, M. Fleischer, F. Schreiber, I. A. Vartanyants and M. Scheele, *Adv. Mater.*, 2020, 2002254.

20 B. Gross, S. Philipp, E. Josten, J. Leliaert, E. Wetterskog, L. Bergström and M. Poggio, *Phys. Rev. B*, 2021, **103**, 014402.

21 M. R. Jones, R. J. Macfarlane, A. E. Prigodich, P. C. Patel and C. A. Mirkin, *J. Am. Chem. Soc.*, 2011, **133**, 18865–18869.

22 J. G. Donaldson, P. Linse and S. S. Kantorovich, *Nanoscale*, 2017, **9**, 6448–6462.

23 L. Rossi, J. G. Donaldson, J.-M. Meijer, A. V. Petukhov, D. Kleckner, S. S. Kantorovich, W. T. M. Irvine, A. P. Philipse and S. Sacanna, *Soft Matter*, 2018, **14**, 1080–1087.

24 S. Disch, E. Wetterskog, R. P. Hermann, G. Salazar-Alvarez, P. Busch, T. Brückel, L. Bergström and S. Kamali, *Nano Lett.*, 2011, **11**, 1651–1656.

25 S. Disch, E. Wetterskog, R. P. Hermann, D. Korolkov, P. Busch, P. Boesecke, O. Lyon, U. Vainio, G. Salazar-Alvarez, L. Bergström and T. Brückel, *Nanoscale*, 2013, **5**, 3969–3975.

26 E. Wetterskog, A. Klapper, S. Disch, E. Josten, R. P. Hermann, U. Rücker, T. Brückel, L. Bergström and G. Salazar-Alvarez, *Nanoscale*, 2016, **8**, 15571–15580.

27 L. Rossi, V. Soni, D. J. Ashton, D. J. Pine, A. P. Philipse, P. M. Chaikin, M. Dijkstra, S. Sacanna and W. T. M. Irvine, *Proc Natl Acad Sci USA*, 2015, **112**, 5286–5290.

28 J.-M. Meijer, A. Pal, S. Ouhajji, H. N. W. Lekkerkerker, A. P. Philipse and A. V. Petukhov, *Nat Commun*, 2017, **8**, 14352.

29 J. Muro-Cruces, A. G. Roca, A. López-Ortega, E. Fantechi, D. del-Pozo-Bueno, S. Estradé, F. Peiró, B. Sepúlveda, F. Pineider, C. Sangregorio and J. Nogues, *ACS Nano*, 2019, **13**, 7716–7728.

30 E. Josten, M. Angst, A. Glavic, P. Zakalek, U. Rücker, O. H. Seeck, A. Kovács, E. Wetterskog, E. Kentzinger, R. E. Dunin-Borkowski, L. Bergström and T. Brückel, *Nanoscale Horiz.*, 2020, **5**, 1065–1072.

31 D. J. Audus, A. M. Hassan, E. J. Garboczi and J. F. Douglas, *Soft Matter*, 2015, **11**, 3360–3366.

32 Y. Jiao, F. Stillinger and S. Torquato, *Phys. Rev. E*, 2009, **79**, 041309.

33 R. D. Batten, F. H. Stillinger and S. Torquato, *Phys. Rev. E*, 2010, **81**, 061105.

34 R. Ni, A. P. Gantapara, J. de Graaf, R. van Roij and M. Dijkstra, *Soft Matter*, 2012, **8**, 8826.

35 P. Linse, *Soft Matter*, 2015, **11**, 3900–3912.

36 J. G. Donaldson, E. S. Pyanzina and S. S. Kantorovich, *ACS Nano*, 2017, **11**, 8153–8166.

37 J.-M. Meijer, D. V. Byelov, L. Rossi, A. Snigirev, I. Snigireva, A. P. Philipse and A. V. Petukhov, *Soft Matter*, 2013, 10.

38 J. R. Royer, G. L. Burton, D. L. Blair and S. D. Hudson, *Soft Matter*, 2015, **11**, 5656–5665.

39 T. Li, A. J. Senesi and B. Lee, *Chem. Rev.*, 2016, **116**, 11128–11180.

40 Y. Zhang, F. Lu, D. van der Lelie and O. Gang, *Phys. Rev. Lett.*, 2011, **107**, 135701.

41 F. Dekker, B. Kuipers, A. Petukhov, R. Tuinier and A. Philipse, *Journal of Colloid and Interface Science*, 2020, **571**, 419–428.

42 *SasView, https://www.sasview.org/*.

43 F. W. J. Olver, D. W. Lozier, R. F. Boisvert and C. W. Clark, *NIST Handbook of Mathematical Functions*, Cambridge University Press, 1st edn, 2010.

44 E. Wetterskog, M. Agthe, A. Mayence, J. Grins, D. Wang, S. Rana, A. Ahniyaz, G. Salazar-Alvarez and L. Bergström, *Science and Technology of Advanced Materials*, 2014, **15**, 055010.

45 J. Park, K. An, Y. Hwang, J.-G. Park, H.-J. Noh, J.-Y. Kim, J.-H. Park, N.-M. Hwang and T. Hyeon, *Nature Mater*, 2004, **3**, 891–895.

46 Jülich Center for Neutron Science, *JLSRF*, 2016, **2**, A61.

47 S. Disch, R. P. Hermann, E. Wetterskog, A. A. Podlesnyak, K. An, T. Hyeon, G. Salazar-Alvarez, L. Bergström and T. Brückel, *Phys. Rev. B*, 2014, **89**, 064402.

48 E. Wetterskog, C.-W. Tai, J. Grins, L. Bergström and G. Salazar-Alvarez, *ACS Nano*, 2013, **7**, 7132–7144.

49 M. A. Roldan, A. Mayence, A. López-Ortega, R. Ishikawa, J. Salafranca, M. Estrader, G. Salazar-Alvarez, M. Dolors Baró, J. Nogués, S. J. Pennycook and M. Varela, *Chemical Engineering Journal*, 2021, **405**, 126820.